

**Structural, electronic, and magnetic properties of SrRuO<sub>3</sub> under epitaxial strain**A. T. Zayak,<sup>1,\*</sup> X. Huang,<sup>2</sup> J. B. Neaton,<sup>3</sup> and Karin M. Rabe<sup>1</sup><sup>1</sup>*Department of Physics and Astronomy, Rutgers University, Piscataway, New Jersey 08854-8019, USA*<sup>2</sup>*RJ Mears, LLC, 1100 Winter Street, Suite 4700, Waltham, Massachusetts 02451, USA*<sup>3</sup>*The Molecular Foundry, Material Sciences Division, Lawrence Berkeley National Laboratory, Berkeley, California 94720, USA*

(Received 24 May 2006; published 20 September 2006)

Using density functional theory within the local spin density approximation, the structural, electronic, and magnetic properties of SrRuO<sub>3</sub> are investigated. We examine the magnitude of the orthorhombic distortion in the ground state and also the effects of applying epitaxial constraints, whereby the influence of large (in the range of  $\pm 4\%$ ) in-plane strain resulting from coherent epitaxy, for both [001] and [110] oriented films, has been isolated and investigated. The overall pattern of the structural relaxations reveals coherent distortions of the oxygen octahedron network, which determine the stability of the magnetic moment on the Ru ion. The structural and magnetic parameters exhibit substantial changes, allowing us to discuss the role of symmetry and possibilities of magnetostructural tuning of SrRuO<sub>3</sub>-based thin-film structures.

DOI: [10.1103/PhysRevB.74.094104](https://doi.org/10.1103/PhysRevB.74.094104)

PACS number(s): 61.66.-f, 75.30.-m, 75.70.Ak, 68.55.-a

**I. INTRODUCTION**

Epitaxial thin-film technology has the potential to change the functionality of conventional crystals in a way to achieve better performance and novel properties. Grown layer by layer in thin-film geometries, the crystals still retain their bulklike properties in two in-plane lateral dimensions, while being strongly modified along the direction of growth by finite-size effects, the presence of interfaces and surfaces, and the misfit strain from epitaxial lattice matching. Additional interactions which emerge between consequent layers allow control, tuning, and enhancing of their functional properties. Complex artificially designed highly oriented heterostructures with specific characteristics can be synthesized with atomic-level precision.<sup>1,2</sup>

In many perovskite-oxide-based heterostructures and superlattices, the metallic ferromagnetic perovskite SrRuO<sub>3</sub> plays a particularly key role, often serving as an electrode material that allows for better integration and facilitates electrical measurements.<sup>3,4</sup> However, recent studies of epitaxial thin films<sup>5</sup> suggest that SrRuO<sub>3</sub> may have novel magnetostructural properties in ultrathin-film form. By tuning the film thickness and in-plane strain (through the choice of substrate) very different properties may emerge as compared with the bulk. Similar approaches have been exploited in recent experimental and theoretical investigations showing modifications of the ferroelectric epitaxial thin films with strongly enhanced performance.<sup>6-9</sup> However, to our knowledge, the impact of strain on ferromagnetic perovskite films has not yet been studied.

Bulk SrRuO<sub>3</sub> undergoes a series of phase transformations with decreasing temperature (for more details see Refs. 10 and 11). It is a metallic ferromagnet with a Curie temperature about 160 K and a magnetic moment of  $1.1\mu_B$  per formula unit.<sup>12</sup> The ideal cubic perovskite structure with cubic symmetry  $Pm\bar{3}m$  is stable above 950 K. From this temperature and down to 820 K it appears in the tetragonal  $I4/mcm$  structure. Below 850 K and at standard pressures, SrRuO<sub>3</sub> has an orthorhombically distorted perovskite structure [space group  $Pbnm$  (Ref. 13) with 20 atoms per cell<sup>15</sup>]. The struc-

ture is the GdFeO<sub>3</sub>/CaTiO<sub>3</sub> type, which can be understood by first doubling the five-atom cell along [110], with both oxygen octahedra being rotated in the same way around [001] ( $z$  axis), and then doubling this ten-atom system along [001], with two oxygen octahedra connected along the  $z$  axis, being further tilted in opposite directions. This structure is shown in Fig. 1. In Glazer notation, the tilting of SrRuO<sub>3</sub> is described by  $(a^-a^-c^+)$ .<sup>16,17</sup> One of our main points below will be that in SrRuO<sub>3</sub>, the rotation and tilting is accompanied by a substantial deformation of the oxygen octahedra.

Previous first-principles studies of SrRuO<sub>3</sub> examined the electronic and magnetic properties of the bulk low-temperature  $Pbnm$  structure.<sup>18-20</sup> Their results largely agree with experimental observations and explain basic features of the ground state in the absence of strain. In this paper, we use first-principles calculations to isolate and investigate the effect of epitaxial strain on the structure of SrRuO<sub>3</sub>. We explore SrRuO<sub>3</sub> with this constraint through examination of the orthorhombic distortion and magnetic and electronic properties of the  $Pbnm$  structure, elucidating the differences between bulk and epitaxially strained thin films in the [001] and [110] orientations.

In Sec. II we give a short description of our methods used in this work. Section III presents our most important results, which we split into two parts. In part A we concentrate on the structural parameters of a strain-free structure and highlight a confusion in the literature about the lattice parameters of SrRuO<sub>3</sub>. Part B deals with [001]- and [110]-oriented structures of SrRuO<sub>3</sub> grown with tensile and compressive misfit strain. Section IV presents discussions of three selected topics which follow from our results and deserve more attention. Conclusions are given in Sec. V.

**II. METHODS**

All calculations are performed with the Vienna *ab initio* simulations package (VASP),<sup>21,22</sup> with the Ceperley-Alder parametrization of the local spin density approximation (LSDA) and projector-augmented-wave potentials.<sup>23,24</sup> The calculations are performed using a plane-wave energy cutoff

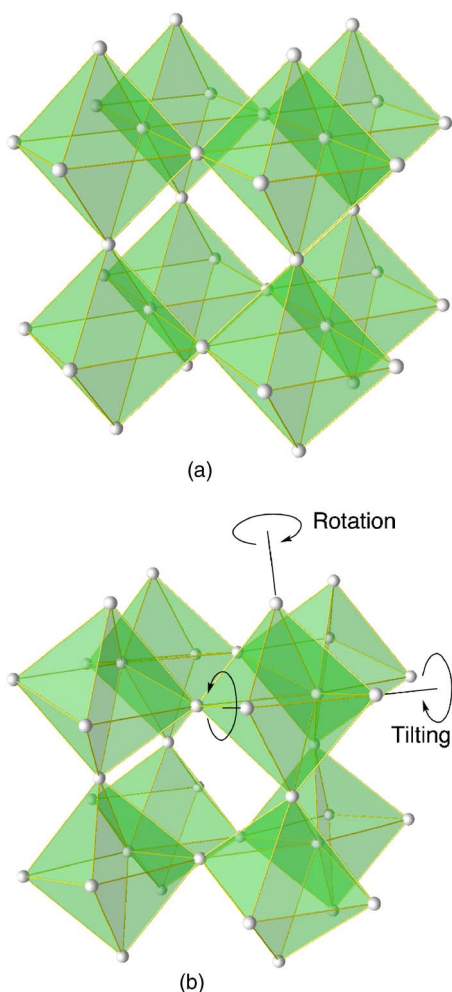


FIG. 1. (Color online) (Top) The structure of the oxygen network in a  $Pm\bar{3}m$  perovskite structure. The oxygen octahedra are perfectly regular. (Bottom) The structure of orthorhombic  $Pbnm$  perovskite structure with tilting (rotation of the octahedral cages). The oxygen octahedra in this case are not necessary regular. We consider this aspect in Sec. III of this paper.

of 500 eV, and the convergence was checked with a cutoff of 600 eV. For calculations with the  $Pbnm$  unit cell of  $\text{SrRuO}_3$ , which contains 4 formula units (f.u.) or 20 atoms per cell, a  $12 \times 12 \times 10$  Monkhorst-Pack  $k$ -point mesh is found to yield convergence of all properties computed here and is used in all self-consistent calculations. For a simple cubic perovskite cell with 5 atoms we used a  $12 \times 12 \times 12$   $k$ -point sampling.

In order to isolate the effects of epitaxial strain, we perform bulk calculations of the  $Pbnm$  ground-state structure with lattice vectors constrained to match a hypothetical substrate. Specifically, for a series of values of misfit strain, we fix the in-plane ( $xy$  plane) lattice vectors, allowing the  $c$  lattice parameter (perpendicular to the substrate) and the internal ionic coordinates to fully relax within the symmetry of the  $Pbnm$  space group. The ions were free to move until the Hellmann-Feynman forces were less than  $4 \text{ meV}/\text{\AA}$ .

Two different angles characterize the degree of rotation and tilting of the oxygen octahedra in  $\text{SrRuO}_3$ . The rotation and tilting represent basically the same type of distortion, but

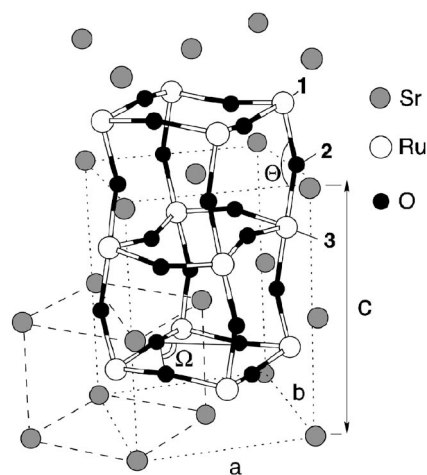


FIG. 2. The  $Pbnm$  crystal structure of  $\text{SrRuO}_3$  ( $\text{GdFeO}_3/\text{CaTiO}_3$  type). The unit cell consists of four formula units of the ideal cubic perovskite structure. The Ru atoms possess relatively large magnetic moments and occupy high-symmetry positions in the orthorhombic unit cell. The atoms of oxygen and Sr are displaced from their high-symmetry positions due to the tilting. The numbers attached to certain atoms help us to define the angle of tilting as discussed in Sec. II.

with respect to different directions. It is conventional to define the rotation along the  $z$  axis separately from those along the  $x$  and  $y$  axes, referred to as tiltings. For what follows, we define the dihedral angle  $\Theta$  to be along the  $\text{Ru}_1\text{-O}_2\text{-Ru}_3$  bond shown in Fig. 2 and the tilting angle is given by  $(180^\circ - \Theta)/2$ . Similarly, the rotation angle is defined through the relation  $(90^\circ - \Omega)/2$ , where  $\Omega$  is an angle shown in Figs. 2 and 3. The rotation and tilting commute with each other and uniquely describe the network of oxygen octahedra, assuming the octahedrons are regular. We will return to the validity of this assumption later in Sec. III.<sup>25</sup>

### III. RESULTS

#### A. Strain-free structure of $\text{SrRuO}_3$

Starting from the experimental space group  $Pbnm$ , we first obtain the ground-state structure of  $\text{SrRuO}_3$  by relaxing all seven free internal structural parameters (internal atomic coordinates) and three lattice parameters. Our results, along with a comparison with the experimental values for different perovskite systems, are shown in Tables I and II. The calculated parameters are in good agreement with experiment. The slight underestimate of the lattice constant is typical for the LSDA.

From Tables I and II, we can see that most of the  $Pbnm$   $\text{GdFeO}_3$ -type structures have  $a < b < c$ . Interestingly, however, in the case of  $\text{SrRuO}_3$  this relation is not satisfied.  $\text{SrRuO}_3$  is the only compound we know of for which this is the case. This has led to a confusion in the literature where one can find reports both of  $a > b$  (see Refs. 11, 15, and 32–34) and  $a < b$  (see Refs. 35–38); in the latter case, parameters are apparently switched to be consistent with overall trend in the  $\text{GdFeO}_3$ -type structures. To clarify the unique

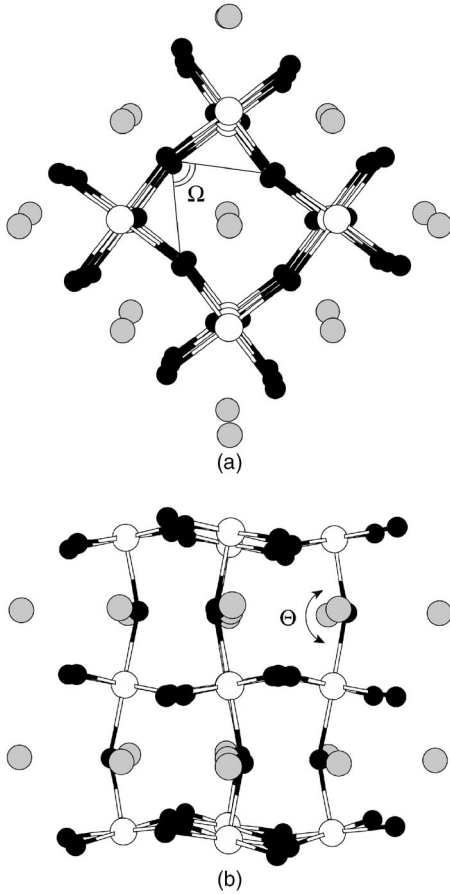


FIG. 3. (Top) The top view of the structure of  $\text{SrRuO}_3$  showing the distortion which we refer to as a rotation. The corner-connected oxygen octahedra rotate in opposite directions around the  $[001]$  direction. This distortion changes the  $a$  and  $b$  parameters of the structure equally. (Bottom) The tilting of the  $\text{SrRuO}_3$  structure shown projected along the  $[110]$  direction (or  $b$  axis of the  $Pbnm$  structure). In this view one can see the folding of the  $[001]$  plane that is responsible for the shrinking of the  $Pbnm$  structure along the  $a$  axis.

situation in  $\text{SrRuO}_3$  other geometrical factors making up the orthorhombic distortions of the  $Pbnm$  structure need to be considered, as we now explain.

Figure 3, together with the sketch in Fig. 4, illustrates the relationship between octahedral tilting and rotation and the orientations of the interatomic bonds. The in-plane lattice parameters of the  $Pbnm$  structure are not equal—that is,  $a \neq b$ —as a consequence of the tilting; the rotation, on the other hand, does not change the ratio of  $a$  to  $b$ . For arrangements with  $Pbnm$  symmetry, if the octahedra were regular, tilting would require  $a < b$ , and not the other way around. This simple geometrical picture explains the orthorhombic shape of most of the known perovskite systems listed in Table I, with the notable exception of  $\text{SrRuO}_3$ .

Our theoretical calculations confirm that for  $\text{SrRuO}_3$ ,  $a > b$  (see Table II), while for the systems like  $\text{CaRuO}_3$  and  $\text{CaTiO}_3$ ,  $a < b$ . An analysis of the results of our calculations shows that the reason for the apparent anomaly in  $\text{SrRuO}_3$  is that the oxygen octahedra are not regular: the “horizontal” middle plane is not square, but rather is rectangular. The

rectangular distortion occurs along the  $b$  axis, partially compensating the orthorhombic distortion originating with the tilting. Thus, two different contributions determine the orthorhombic distortion (the  $a/b$  ratio) in the  $Pbnm$  structure.

In Table II we summarize the impact of distortions coming from each contribution. The anomalous orthorhombic distortion in  $\text{SrRuO}_3$  is derived from geometrical considerations and those parameters which we already have:  $a$ ,  $b$ ,  $c$ , and tilting and rotation angles. If  $a^{\text{oct}}$  and  $b^{\text{oct}}$  describe the equatorial plane of the octahedra, then the lattice parameters of  $Pbnm$  can be expressed as follows:

$$\begin{cases} a = 2a^{\text{oct}} \cos(\text{rotation})\cos(\text{tilting}), \\ b = 2b^{\text{oct}} \cos(\text{rotation}). \end{cases} \quad (1)$$

Consequently, the orthorhombic distortion can be expressed as

$$\frac{a}{b} = \left[ \frac{a^{\text{oct}}}{b^{\text{oct}}} \right] \cos(\text{tilting}). \quad (2)$$

These simple relations show that the internal distortions can be readily determined from fundamental parameters of the  $Pbnm$  structure. However, it is important to note that the oxygen octahedra are not necessarily regular; i.e.,  $a^{\text{oct}}$  and  $b^{\text{oct}}$  are free parameters unique for each material.

### B. Magnetic properties of strain-free $\text{SrRuO}_3$

We calculate the FM state in  $Pbnm$  structure to have an energy 186 meV/f.u. lower than that of the cubic perovskite FM system, which was optimized within the  $Pm\bar{3}m$  symmetry (see Table III). A previous first-principles study (Ref. 18) computed a comparable energy difference, 140 meV/f.u., using structures with experimental lattice parameters.

Experimental values of the magnetic moment in  $\text{SrRuO}_3$  range between  $1.1\mu_B/\text{f.u.}$  and  $1.6\mu_B/\text{f.u.}$ ; the spread in values is expected given the difficulty of making single-domain samples and their large magnetocrystalline anisotropy.<sup>12,25</sup> According to Ref. 20, only approximately 60% of the total magnetic moment is Ru derived, while the remaining 40% is distributed among oxygen sublattice sites. A similar spread of the values of the magnetic moment in  $\text{SrRuO}_3$  has been reported from theoretical investigations. Usually they are obtained using the LSDA and experimental lattice parameters for the orthorhombic  $Pbnm$  structure. Such calculations reported magnetic moments ranging between  $0.97\mu_B/\text{f.u.}$  and  $1.96\mu_B/\text{f.u.}$ <sup>18,19,36,39</sup>

With an intermediate degree of relaxation, keeping the experimental lattice parameters fixed, but allowing the Wyckoff positions to change, we obtain  $1.2\mu_B/\text{f.u.}$  After a complete relaxation of the structure, our magnetic moment calculated with the LSDA is  $0.98\mu_B/\text{f.u.}$ , smaller than that obtained with experimental lattice parameters, as would be expected with the smaller LSDA lattice parameters. A summary of all calculated lattice parameters appears in Table II. The LSDA slightly overestimates the bond strength and therefore favors stronger hybridization of the Ru  $d$  and O  $p$  states, giving smaller lattice parameters and consequently smaller magnetic moments.

TABLE I. Experimental structural parameters for several perovskite systems with  $Pbnm$  symmetry taken from Refs. 15 and 27–31. We focus in this list on the relations of the  $a$ ,  $b$ , and  $c$  lattice parameters. In most of the systems  $a < b$  is satisfied due to the tilting of the oxygen octahedra, whereby only the  $a$  vector shrinks, while the  $b$  vector remains unchanged. From this table, one can see that for  $\text{SrRuO}_3$  the ratio  $a < b$  is not satisfied.

	$a$ (Å)	$b$ (Å)	$c$ (Å)	Wyckoff position	$x$	$y$	$z$
$\text{SrRuO}_3$	5.5670	5.5304	7.8446	Sr (4c)	-0.0027	0.0157	0.25
				Ru (4b)	0.5	0.0	0.0
				O (8d)	0.7248	0.2764	0.0278
				O (4c)	0.0532	0.4966	0.25
$\text{GdFeO}_3$	5.3510	5.6125	7.6711	Gd (4c)	-0.0015	0.0626	0.25
				Fe (4b)	0.5	0.0	0.0
				O (8d)	0.6966	0.3011	0.0518
				O (4c)	0.1009	0.4669	0.25
$\text{GdAlO}_3$	5.2537	5.3030	7.4434	Gd (4c)	-0.0079	0.0376	0.25
				Al (4b)	0.5	0.0	0.0
				O (8d)	0.7147	0.2855	0.0387
				O (4c)	0.0724	0.4863	0.25
$\text{CaTiO}_3$	5.3804	5.4422	7.6417	Ca (4c)	-0.0065	0.0349	0.25
				Ti (4b)	0.5	0.0	0.0
				O (8d)	0.7111	0.2884	0.0372
				O (4c)	0.0707	0.4842	0.25
$\text{CaRuO}_3$	5.3408	5.5311	7.6460	Ca (4c)	-0.0150	0.0560	0.25
				Ru (4b)	0.5	0.0	0.0
				O (8d)	0.6930	0.2970	0.0530
				O (4c)	0.0910	0.4670	0.25
$\text{GdScO}_3$	5.4862	5.7499	7.9345	Gd (4c)	-0.0163	0.0594	0.25
				Sc (4b)	0.5	0.0	0.0
				O (8d)	0.6931	0.3007	0.0556
				O (4c)	0.1183	0.4465	0.25
$\text{DyScO}_3$	5.4400	5.7130	7.887	Dy (4c)	-0.0172	0.0607	0.25
				Sc (4b)	0.5	0.0	0.0
				O (8d)	0.6926	0.3040	0.0608
				O (4c)	0.1196	0.445	0.25

In addition to the ferromagnetic (FM) configuration, we optimize the bulk structural parameters of  $\text{SrRuO}_3$  with different initial magnetic orderings, including the nonmagnetic (NM) phase and three different antiferromagnetic (AFM) spin arrangements. Several local minima in the total energy are found. Among these minima, the FM configuration is computed to be the most stable state, in agreement with experiment. The  $A$ -type AFM and  $C$ -type AFM and NM configurations are found to be 6.77 meV/f.u., 6.44 meV/f.u., and 8.15 meV/f.u. higher in energy than the FM ground state, respectively. The  $G$ -type AFM configuration is found to be unstable: when relaxed, it reverts to the NM minimum. In the remainder of this paper, we focus on the FM state and its comparison with the NM state.

### C. Epitaxially constrained structure: $e$ - $Pbnm$

We now consider the structure and properties of epitaxially strained  $Pbnm$   $\text{SrRuO}_3$ . Experimentally,  $\text{SrRuO}_3$  films

can grow with either [001] or [110] orientations on various substrates like  $\text{LaAlO}_3$ ,  $\text{SrTiO}_3$ ,  $\text{DyScO}_3$ , or  $\text{GdScO}_3$  (Refs. 34 and 38) (see Ref. 37 for good illustrations of the two geometries). The [001] case is a relatively straightforward extension of previously studied perovskite multilayers,<sup>40,41</sup> except that additional degrees of freedom must be considered to account for the tilting and rotation. In the [110] orientation, the situation is quite different, as we discuss in detail below.

#### 1. Geometries of the [001]- and [110]-oriented films

For the [001]-oriented films, the  $a$  and  $b$  parameters of the orthorhombic  $Pbnm$  lattice are constrained to be equal (in order to match the square lattice of the substrate). We refer to these constrained structures, with all other structural parameters relaxed, as  $e$ - $Pbnm$  [001], where “ $e$ ” indicates “epitaxial.” Misfit strain is measured relative to the lowest energy  $e$ - $Pbnm$  [001] structure, the computed parameters being given in Table III. Note that the zero-misfit-strain structure is not

TABLE II. Calculated structural parameters for several perovskite systems with  $Pbnm$  symmetry. Theoretical results also show the distortion of  $\text{SrRuO}_3$  for which the orthorhombic distortion is opposite to other perovskites. We introduce the parameters  $\Delta a$  and  $\Delta b$ , which characterize shrinking of the  $a$  and  $b$  lattice parameters, respectively. The parameter  $a$  shrinks due to the tilting, while  $b$  shrinks due to the rectangular distortion of the horizontal middle plane of the oxygen octahedra.

	$a$ (Å)	$b$ (Å)	$c$ (Å)	Wyckoff position	$x$	$y$	$z$	Tilting	$\Delta a$	$\Delta b$
$\text{SrRuO}_3$	5.5031	5.4828	7.7546	Sr (4c)	-0.0050	0.0296	0.25	10.21°	1.58	1.75
				Ru (4b)	0.5	0.0	0.0			
				O (8d)	0.7165	0.2834	0.0336			
				O (4c)	0.0647	0.4941	0.25			
$\text{CaRuO}_3$	5.2090	5.5297	7.5512	Ca (4c)	-0.0211	0.0645	0.25	16.79°	4.26	2.15
				Ru (4b)	0.5	0.0	0.0			
				O (8d)	0.6929	0.2996	0.0519			
				O (4c)	0.1034	0.4665	0.25			
$\text{CaTiO}_3$	5.2900	5.4007	7.5334	Ca (4c)	-0.0099	0.0468	0.25	13.26°	2.67	0.75
				Ti (4b)	0.5	0.0	0.0			
				O (8d)	0.7065	0.2926	0.0425			
				O (4c)	0.0811	0.4790	0.25			

the same as the strain-free structure discussed in the previous subsection, as the latter is not compatible with the epitaxial constraints. For the  $e$ - $Pbnm$  structure we have  $\Delta a = \Delta b$  (from Table II); i.e., two kinds of distortions compensate each other, as they are forced to by the imposed conditions.

In the [110] orientation, we consider a general case when the  $\text{SrRuO}_3$  film is grown on an orthorhombic substrate. We assume that our substrate has in-plane nonequal lattice parameters, but they are kept orthogonal. If we made the in-plane parameters equal, this would correspond, for example, to a cubic lattice of  $\text{SrTiO}_3$  with a compressive lattice mismatch of about 0.59%. But making the in-plane lattice rect-

angular brings us close to the situation with  $\text{GdScO}_3$  or  $\text{DyScO}_3$  substrates, whose structures match nicely with the [110]-oriented structure of  $\text{SrRuO}_3$  (we refer to it as  $e$ - $Pbnm$  [110], although we show that it may have lower symmetry). In this case  $\text{SrRuO}_3$  is subject to substantially different constraints compared with the [001] orientation. The diagonal  $\sqrt{a^2 + b^2}$  is fixed and the lattice parameter  $c$  is the in-plane parameter. The out-of-plane lattice vector is not perpendicular to the surface (see Fig. 5), because its angle with the normal to the surface is given by the difference between the parameters of  $Pbnm$ ,  $a$  and  $b$ :

$$\gamma = 2 \arctan\left(\frac{b}{a}\right) = 2 \arctan\left(\frac{b^{\text{oct}}}{a^{\text{oct}}} \cos(\text{tilting})\right). \quad (3)$$

Although the diagonal  $\sqrt{a^2 + b^2}$  is fixed on the substrate, the ratio  $a/b$  is free to change. From Eq. (1) we see that  $b/a = (b^{\text{oct}}/a^{\text{oct}}) \cos(\text{tilting})$ . At zero in-plane strain the [110]-oriented  $\text{SrRuO}_3$  retains the bulk structure if it is grown on  $\text{SrTiO}_3$ , but not in the case of [001]-oriented  $\text{GdScO}_3$  or  $\text{DyScO}_3$  substrates.

## 2. Structural changes as a function of strain

As the epitaxial constraint is varied, the shape of the cell is changed, which increases its internal energy. In Fig. 6, we plot the elastic energy of ferromagnetic  $\text{SrRuO}_3$  for misfit strains ranging from -4.5% to +3.5%. Surprisingly, the energetic penalties for the in-plane distortion are nearly the same for both  $e$ - $Pbnm$  and  $P4/mmm$  structures, though the latter has no internal degrees of freedom to relax and reduce the energy. Moreover, comparing these curves with another perovskite  $\text{CaTiO}_3$ , we see that their behavior is strikingly similar. Changes of the volume are shown in Fig. 7, below.

The degree of tilting and rotation of the oxygen octahedra reflects the impact of epitaxial strain. Figure 9, below, shows the evolution of these angles for both [001] and [110] orientations. For [110] the two angles decrease together. On the other hand, for the [001] orientation, the angles behave op-

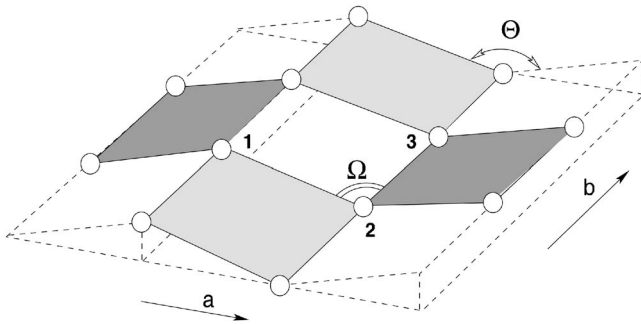


FIG. 4. This picture illustrates schematically the fact that as a result of tilting the  $Pbnm$  structure is necessarily orthorhombic. This appears from simple geometrical considerations when tiltings  $a^-a^-$  have the effect of folding of the Ru-O (001) atomic planes. If the folding develops along the  $a$  axis, while another lattice vector  $b$  remains unchanged, we have  $a < b$ . The importance of this point can be seen when the  $Pbnm$  structure is subject to the epitaxial constraints enforcing  $a=b$ . The rotation around the  $z$  axis is different because it changes the  $a$  and  $b$  parameters of the  $Pbnm$  structure in equal proportions. So the  $a=b$  constraint requires the middle plane of the oxygen octahedra to shrink along the  $b$  axis. In order to characterize this epitaxially constrained structure we introduce the notation  $e$ - $Pbnm$ . The angles shown define degrees of tilting and rotation as discussed in Sec. II.

TABLE III. Computed structural parameters of  $\text{SrRuO}_3$  in the cubic perovskite (space group  $Pm\bar{3}m$ ) and the epitaxially constrained structure  $e\text{-}Pbnm$  [001] in the zero-strain state. Results for both FM and NM configurations are listed in order to show that they do not have significant differences (later on, it will be shown that applying epitaxial strain yields important differences between the FM and NM cases). The Wyckoff positions for all structures refer to space group  $Pbnm$ .

	$a$ (Å)	$b$ (Å)	$c$ (Å)	Wyckoff position	$x$	$y$	$z$	Tilting	$\Delta a$	$\Delta b$
$e\text{-}Pbnm(\text{FM})$	5.4929	5.4929	7.7514	Sr (4c)	-0.0055	0.0303	0.25	$10.48^\circ$	1.67%	1.67%
				Ru (4b)	0.5	0.0	0.0			
				O (8d)	0.7160	0.2837	0.0336			
				O (4c)	0.0650	0.4937	0.25			
$e\text{-}Pbnm(\text{NM})$	5.4929	5.4929	7.7440	Sr (4c)	-0.0051	0.0304	0.25	$10.48^\circ$	1.67%	1.69%
				Ru (4b)	0.5	0.0	0.0			
				O (8d)	0.7155	0.2842	0.0345			
				O (4c)	0.0650	0.4945	0.25			
Cubic(FM)	5.5070	5.5070	7.7880	Sr (4c)	0.0	0.0	0.25	0.0	0.0	0.0
				Ru (4b)	0.5	0.0	0.0			
				O (8d)	0.75	0.25	0.0			
				O (4c)	0.0	0.5	0.25			

positively: for increasing compressive or tensile strain, the rotation or tilting becomes more pronounced, respectively. However, we find that the angles exhibit surprising behavior under tensile strain in the NM state (discussed further below).

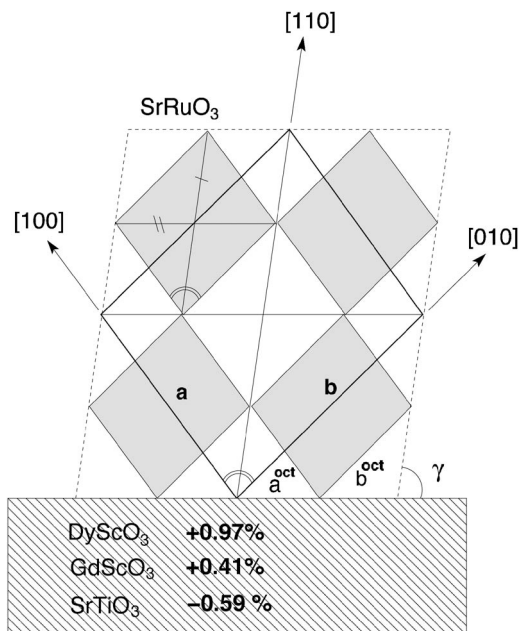


FIG. 5. Schematic presentation of the epitaxial structure of  $\text{SrRuO}_3$  grown in the [110] orientation. The gray parallelograms represent the equatorial planes of the oxygen octahedra in the (001) plane. This geometry implies that at zero in-plane strain the structure still has the orthorhombic symmetry, but its [110] direction is not normal to the substrate. Due to the orthorhombic symmetry, there is an angle  $\gamma$  defined by Eq. (3). Applying in-plane strain changes this angle, but at the same time the orthorhombic symmetry is broken.  $\text{SrRuO}_3$  grown with the [110] orientation under strain is monoclinic.

In addition to the orientation of the oxygen octahedra, we observe that their shape is also changing. This is especially important because we have to understand the behavior of the angles in the NM case shown in Fig. 9. The splitting of two Ru-O $_z$  curves in Fig. 10, below, can be explained by the fact that the NM configuration allows for additional tetragonal contraction of the oxygen octahedra along the  $z$  axis. This contraction manifests itself in the trend in angles shown in Fig. 9. The connection of this effect with the magnetic properties of  $\text{SrRuO}_3$  will be discussed later in Sec. IV.

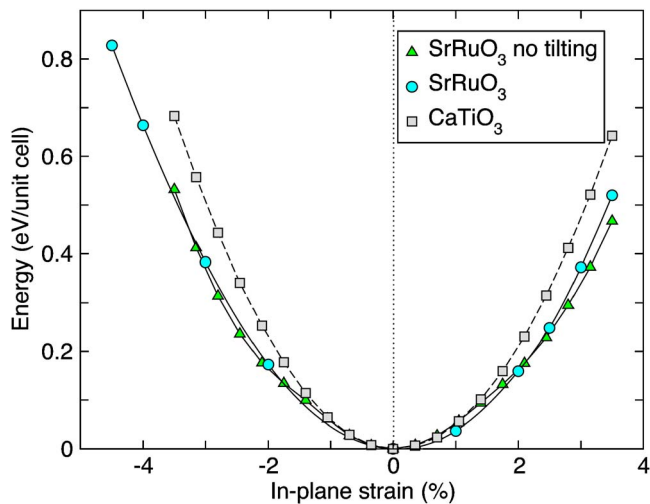


FIG. 6. (Color online) The comparison of the elastic energies of FM  $e\text{-}Pbnm$  [001]  $\text{SrRuO}_3$  and NM  $e\text{-}Pbnm$  [001]  $\text{CaTiO}_3$  as a function of the applied misfit strain. The in-plane lattice parameters were fixed by the value of the misfit strain, while all other parameters of the structures were relaxed to the zero-force states. In addition we show here the total energy of the simple  $P4/mmm$  perovskite  $\text{SrRuO}_3$  when rotation and tilting are not allowed. This allows us to conclude that the tilting does not change the elasticity of the structure with respect to the misfit strain.

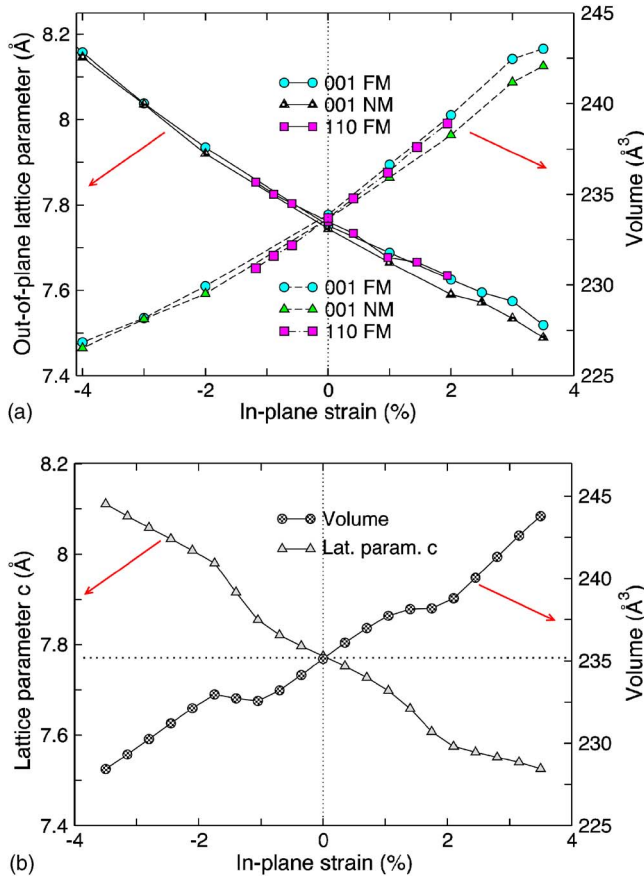


FIG. 7. (Color online) Lattice parameter  $c$  and the volume of the [001]- and [110]-oriented perovskite structures of SrRuO<sub>3</sub> under epitaxial strain. (Top) The epitaxially constrained *e-Pbnm* structure. Both volume change and tetragonal distortion cost energy, whereby the structure changes these degrees of freedom simultaneously. Both [001]- and [110]-oriented films show similar changes in the volume as a function of the strain. (Bottom) Nontilted [001]-oriented simple perovskite *P4/mmm*. Both curves show remarkable difference of their behavior as compared to the *e-Pbnm* structure. A comparison to Fig. 8 shows that the distortions of the *P4/mmm* are strongly influenced by the magnetoelastic coupling.

Applying strain induces a change in volume. In the [110] orientation, the volume can be modified by rotating the angle  $\gamma$  or by expanding (or contracting) the out-of-plane lattice parameter. The latter can be achieved only if the symmetry of the oxygen octahedra is broken. Namely, the middle plane Ru-O bonds would be required to have different length; in the case of [001]-oriented films, they are the same (see Fig. 10). This additional lowering of the symmetry alters the electronic environment of the Ru ion, leading to a drop of its magnetic moment, as shown in Fig. 8, below. The [110]-oriented structure of SrRuO<sub>3</sub> becomes monoclinic<sup>42</sup> (see Fig. 5).

#### IV. DISCUSSIONS

From the results reported above, we selected three particular points for further discussion. Our focus here is on the

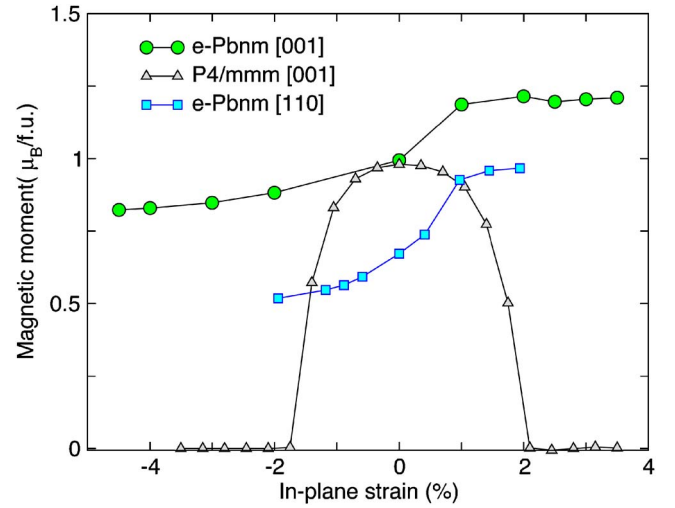


FIG. 8. (Color online) The total magnetic moment of SrRuO<sub>3</sub> as a function of strain. In the case when tilting is not allowed (*P4/mmm*), the deformation of the Ru-O octahedra, occurring due to the strain, becomes so strong that the total magnetic moment drops down to zero. Redistribution of the electron orbitals changes the magnetic interactions. Beyond critical values of the strain, SrRuO<sub>3</sub> becomes nonmagnetic. When the tilting is present (*Pbnm* structure) the magnetic moment is retained even at large in-plane strain. In the [110]-oriented film the magnetic moment is significantly smaller, which we attribute to the geometry of the oxygen cages and the corresponding changes in the electronic structure (see DOS in Fig. 12).

magnetostructural coupling in SrRuO<sub>3</sub> and its dependence on the film orientation.

##### A. Magnetoelastic coupling

Figure 7 (bottom) exhibits some nonlinearity in the volume and out-of-plane lattice parameter of the *P4/mmm* as functions of the misfit strain, in contrast with the almost linear trends in the *e-Pbnm* [001] structure; see Fig. 7 (top). To understand the behavior of the *P4/mmm* structure, it is useful to compare Figs. 7 and 8. Both curves, corresponding to the *P4/mmm* structure, show inflection points in Fig. 7 that coincide with abrupt drops of the magnetic moment in Fig. 8. Evidently, the magnetic moment, via the spin configuration of the Ru ion, stabilizes a symmetrical nondeformed shape of the oxygen octahedra. Concurrently, in-plane strain leads to out-of-plane lattice expansion (contraction) under compressive (tensile) strain. At some critical strain the contraction becomes more favorable than the magnetic orbital ordering and the lattice distorts. On the other hand, in the *e-Pbnm* structure, the tilting and rotation preserve the shape of octahedra and the magnetic orbital ordering survives (see Fig. 9).

The behavior described here suggests a strong magnetostructural interaction, which may potentially explain past experiments showing an anomalous thermal expansion of SrRuO<sub>3</sub>.<sup>29</sup> We reserve a more complete investigation for future work.

##### B. Anomaly of tilting and FM-NM transition

In the previous section we saw the effect of coupling between the distortions of the oxygen octahedra and the stabil-

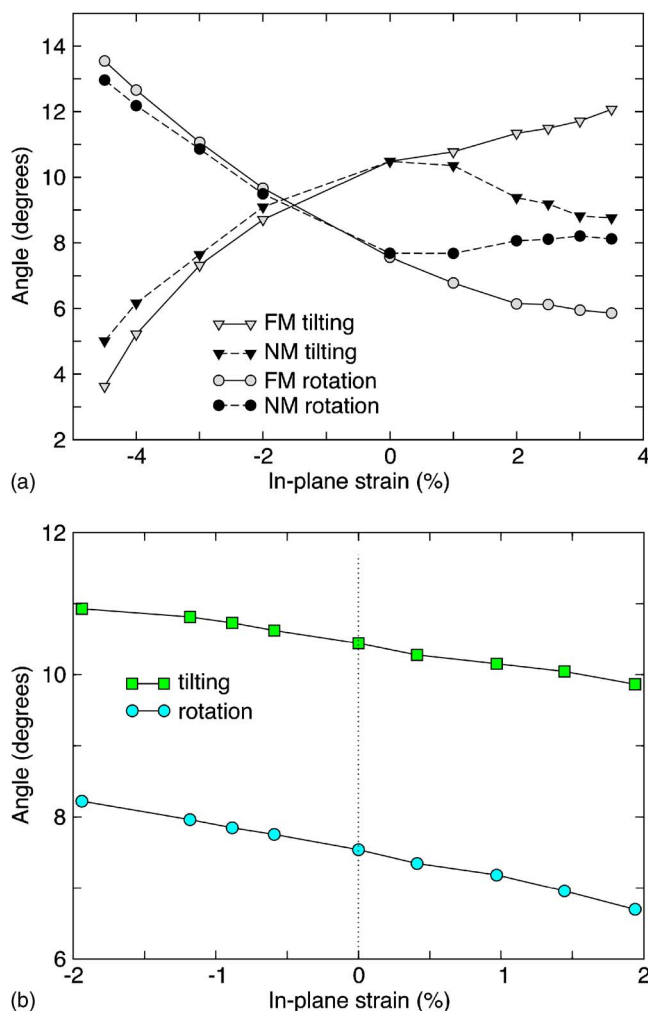


FIG. 9. (Color online) Tilting and rotation angles of the oxygen octahedra as a function of strain. (Top) The  $e\text{-Pbnm}$  [001] structure shows a sudden change in the behavior of the tilting and rotation angles in the NM system, which turns out to be due to the additional contraction of the oxygen octahedra along the  $z$  axis (see Fig. 10). In both the FM and NM cases under tensile strain the rotation angles stay close to a value of  $10^\circ$ . (Bottom) In the  $e\text{-Pbnm}$  [110] orientation, both angles are fixed by the substrate constraint.

ity of the magnetic moment on Ru in the  $P4/mmm$  symmetry. This allows us to understand what we see in the case of  $e\text{-Pbnm}$  [001] structure. In Fig. 10, we see an extra contraction of the Ru-O $z$  bond, which occurs in the NM phase under tensile strain. In contrast, in the FM phase the oxygen octahedra keep their shape by monotonically increasing the tilting angle.

This difference in the behavior of the magnetic and non-magnetic phases can be explained from a simple spin configuration argument known for  $\text{SrRuO}_3$ .<sup>43</sup> If the structure is not distorted, four  $4d$  electrons of  $\text{Ru}^{4+}$  occupy threefold-degenerate  $t_{2g}$  orbitals leading to  $(\uparrow t_{2g}^3, \downarrow t_{2g}^1)$ , whereby two spins are not compensated and the Ru ion has a large magnetic moment. If the oxygen octahedra are contracted along some of the Ru-O bonds, the  $t_{2g}$  orbitals split, producing a nonmagnetic spin configuration for Ru,  $\uparrow t_{2g}^2, \downarrow t_{2g}^2$ .

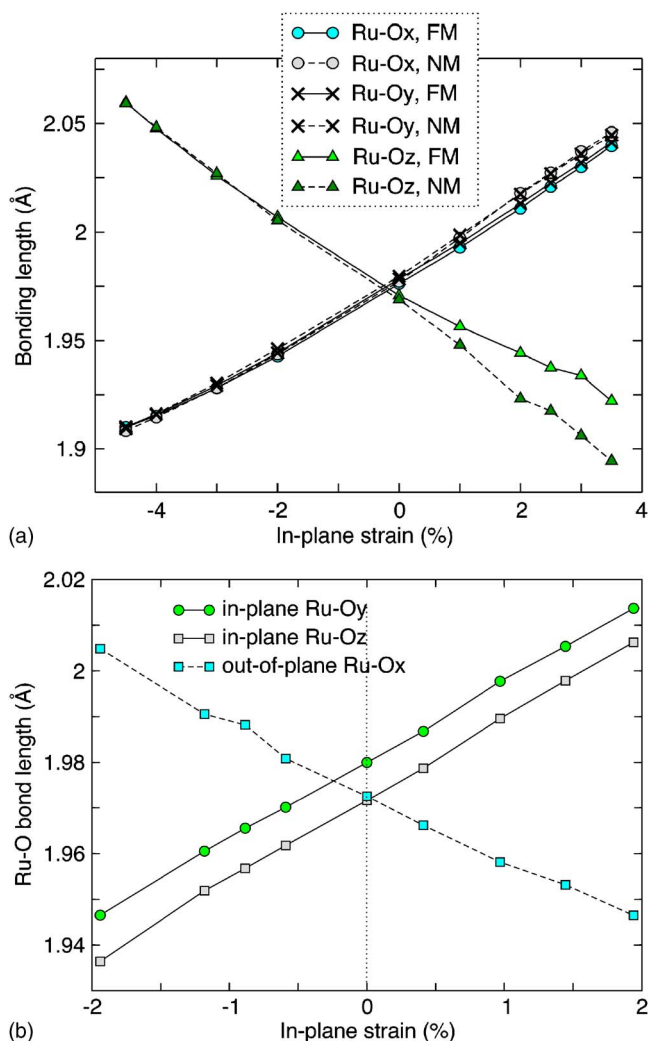


FIG. 10. (Color online) Bond lengths of Ru-O inside the oxygen octahedral cages as functions of in-plane strain. (Top) The [001]-oriented film with FM and NM configurations. Under tensile strain the NM and FM curves split, which is due to the additional contraction of the oxygen octahedra along the  $z$  axis in the NM case, which is reflected in smaller tilting angles shown in Fig. 9. (Bottom) In the [110] orientation, the substrate has an orthorhombic shape; therefore, the in-plane parameters of the  $\text{SrRuO}_3$  film are distorted. In order to be consistent we use the notations of the [001] orientation. Therefore, the  $x$  axis in this case is out of plane.

Such a transition is possible and can have significant implications for the magnetostructural tuning of the  $\text{SrRuO}_3$ -based heterostructures. One could change the magnetic ground state of  $\text{SrRuO}_3$  by using uniaxial compression. Starting from the FM state, one can apply a uniaxial stress along the  $c$  axis. The NM state which has a shorter lattice parameter  $c$  can become the ground state. Some doping of the  $\text{SrRuO}_3$  structure with larger atoms, like Ba, should make tilting weaker and therefore favor the NM state—i.e., reduce the amount of pressure required to transform the structure. We will discuss this issue in more detail with possible applications in our next paper.

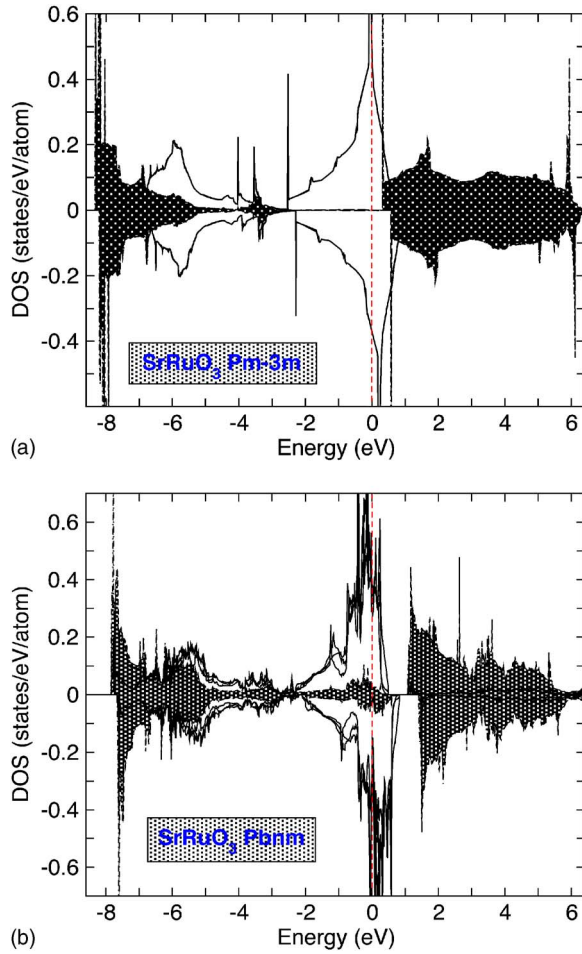


FIG. 11. (Color online) Ru-site-projected partial DOS of SrRuO<sub>3</sub>. The electronic states with  $e_g$  symmetry are filled with gray color. Different orientations of the  $t_{2g}$  and  $e_g$  orbitals are plotted together without distinction in order to focus on the gaps which open when distortions are applied to the structure. (Top) DOS of the simple perovskite structure with  $Pm\bar{3}m$  symmetry. There is no gap above the Fermi level. (Bottom) DOS of the strain free bulk  $Pbnm$  structure. There is a gap above the Fermi level, which opens, as we discuss in the text, due to the rotations of the oxygen octahedra. In Fig. 12 it is shown that in the [110]-oriented structure, one more gap opens.

### C. Orientation dependence

We now comment on the differences between [001]- and [110]-oriented films. For the [001]-oriented films, the oxygen octahedra are free to rotate and tilt, adapting to the changing lattice parameters. In contrast, in the [110] orientation both angles are fixed to the parameters of substrate. Moreover, we stressed above that [110]-oriented SrRuO<sub>3</sub> becomes monoclinic. This difference has consequences for the calculated electronic structure. We show the electronic density of states (DOS) projected on the Ru sites for four different cases. These four plots are intended to illustrate how the electronic environment of Ru changes when distortions of the oxygen cage network occur.

The additional lowering of the symmetry in the [110] orientation leads to a splitting of the  $t_{2g}$  bands associated with

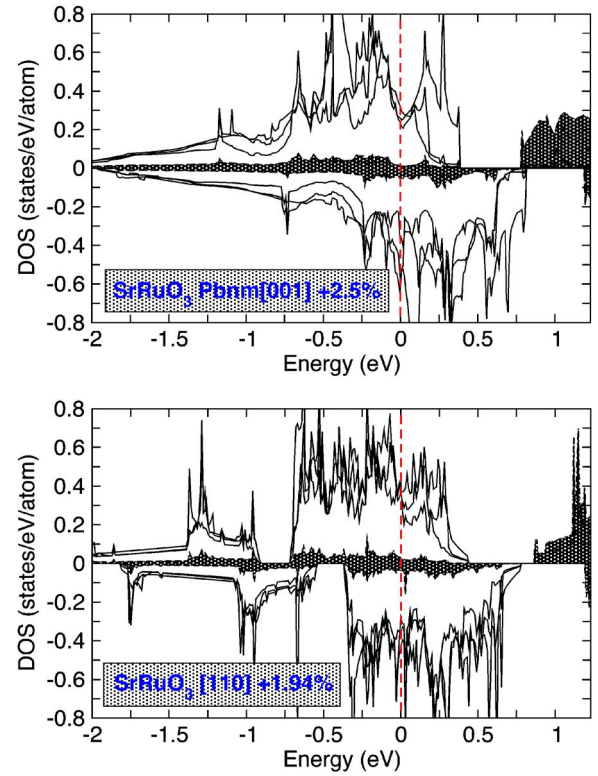


FIG. 12. (Color online) Ru-site-projected partial DOS of SrRuO<sub>3</sub> in the vicinity of  $E_F$ . The electronic states with  $e_g$  symmetry are filled with gray color. Different orientations of the  $t_{2g}$  and  $e_g$  orbitals are plotted together without distinction in order to focus on the gaps which open when distortions are applied to the structure. (Top) DOS for the  $e-Pbnm$  [001] structure of SrRuO<sub>3</sub> under tensile strain of 2.5%. The tensile strain reduces in-plane distortion of the oxygen octahedra, whereby the gap becomes smaller. (Bottom) DOS for the  $e-Pbnm$  [110] structure. The strain is now also tensile, but 1.94%. There is another gap which opens about 0.8 eV (0.4 eV for spin-down states) below the Fermi level. It happens because the [110] orientation required additional distortion of the oxygen cages, forcing the  $t_{2g}$  electrons of Ru to split.

the Ru  $d$  level and a smaller magnetic moment (Fig. 8). The gap opens at about 0.8 eV below  $E_F$  for the spin-up states and 0.4 eV below  $E_F$  for the spin-down component [Fig. 12 (bottom)].

From examination of the electronic structure in Figs. 11 and 12 four additional features emerge. We summarize them as follows: First, for  $Pm\bar{3}m$ , there are no distortions of the oxygen octahedra, and thus there is no gap in the DOS [see Fig. 11 (top)]; second, for  $Pbnm$  the octahedra are rotated, and thus the  $t_{2g}$  and  $e_g$  bands start to “feel” each other and repel, and as a consequence, there is a gap just above  $E_F$  in the DOS [see Fig. 11 (bottom)]; for  $e-Pbnm$  [001] under tensile strain, the rotation is reduced and  $t_{2g}(xy)$  and  $e_g(x^2 - y^2)$  recover their symmetry, whereby their repulsion becomes weaker, reducing the gap above  $E_F$  [see Fig. 12 (top)]. Finally, for  $e-Pbnm$  [110], this orientation requires further lowering of the symmetry. The crystal field splits the  $t_{2g}$  bands and opens an additional gap 0.8 eV (0.4 eV for spin-down states) below the  $E_F$ .

## V. CONCLUSIONS

In this paper, we studied the properties of SrRuO<sub>3</sub> under conditions of epitaxial strain and different thin-film orientations and considered how the changes that take place in SrRuO<sub>3</sub> may be used to tune the properties of SrRuO<sub>3</sub>- and SrRuO<sub>3</sub>-based heterostructures. The results can be summarized as follows.

We explained the mechanism leading to the orthorhombic distortion of *Pbnm*: namely, the tilting and contraction of the oxygen octahedra. The “anomalous” orthorhombic shape of SrRuO<sub>3</sub> can be easily understood from simple geometrical considerations.

Two different orientations of the SrRuO<sub>3</sub> epitaxial films, *e-Pbnm* [001] and *e-Pbnm* [110], exhibit significant differences in their structural properties. The latter, unless there is no in-plane strain, has monoclinic symmetry, while the [001]-oriented film remains orthorhombic at any reasonable value of the strain.

SrRuO<sub>3</sub> exhibits significant magnetostructural coupling. Tensile strain reveals that in the nonmagnetic state there is a

distortion of Ru-O<sub>z</sub> bonds which can be attributed to the change of Ru spin configuration, explaining the fact that this distortion does not appear in the magnetic state. The tilting and rotation help to preserve the shape of the octahedra when epitaxial strain is applied, whereby the magnetic orbital ordering is preserved. By suppressing the tilting under strain one could obtain a nonmagnetic state of SrRuO<sub>3</sub>.

## ACKNOWLEDGMENTS

This work was supported by the NSF (Grant No. MRSEC DMR-00-80008) and DOE Grant No. DE-FG02-01ER45937. Work at the Molecular Foundry was supported by the Director, Office of Science, Office of Basic Energy Sciences, Division of Materials Sciences and Engineering, of the U.S. Department of Energy under Contract No. DE-AC02-05CH11231. We thank E. Liskova, C. J. Fennie, D. Singh, D. Vanderbilt, M. H. Cohen, and D. R. Hamann for their help and discussions. We also thank P. Woodward for helpful feedback and for providing his code POTATO.

\*Electronic address: zayak@physics.rutgers.edu

<sup>1</sup>R. Ramesh and D. G. Schlom, *Science* **296**, 1975 (2002).

<sup>2</sup>H. N. Lee *et al.*, *Nature (London)* **433**, 395 (2005).

<sup>3</sup>K. Maki *et al.*, *Appl. Phys. Lett.* **82**, 1263 (2003).

<sup>4</sup>Z.-G. Ban *et al.*, *Appl. Phys. Lett.* **84**, 4848 (2004).

<sup>5</sup>Q. Gan *et al.*, *Appl. Phys. Lett.* **72**, 978 (1998).

<sup>6</sup>V. Nagarajan *et al.*, *J. Appl. Phys.* **86**, 595 (1999).

<sup>7</sup>D. Fuchs, C. W. Schneider, R. Schneider, and H. Rietschel, *J. Appl. Phys.* **85**, 7362 (1999).

<sup>8</sup>M. E. Lines and A. M. Glass, *Principles and Applications of Ferroelectrics and Related Materials* (Clarendon Press, Oxford, 1977).

<sup>9</sup>A. Antons, J. B. Neaton, K. M. Rabe, and D. Vanderbilt, *Phys. Rev. B* **71**, 024102 (2005).

<sup>10</sup>B. C. Chakoumakos, S. E. Nagler, S. T. Mixture, and H. M. Christen, *Physica B* **241-243**, 358 (1998).

<sup>11</sup>F. He, B. O. Wells, Z.-G. Ban, S. P. Alpay, S. Grenier, S. M. Shapiro, W. Si, A. Clark, and X. X. Xi, *Phys. Rev. B* **70**, 235405 (2004).

<sup>12</sup>A. Kanbayasi, *J. Phys. Soc. Jpn.* **41**, 1876 (1976).

<sup>13</sup>According to crystallographic rules the notation of this space group is *Pnma* which has the doubled *b* axis with respect to the simple perovskite structure. However, the physics community traditionally prefers the *c* axis to be the reference direction; therefore the *Pbnm* is used in this work. These two notations are related via a simple transformation (Ref. 14). For the space group *Pnma* we have the lattice parameters  $a_1 \sim \sqrt{2}a_p$ ,  $b_1 \sim 2a_p$ , and  $c_1 \sim \sqrt{2}a_p$ , where  $a_p$  is the lattice parameter of the cubic perovskite structure. Space group *Pbnm* has lattice parameters  $a_2 \sim \sqrt{2}a_p$ ,  $b_2 \sim \sqrt{2}a_p$ , and  $c_2 \sim 2a_p$ . The transformation from *Pnma* to *Pbnm* is  $a_1 \rightarrow b_2$ ,  $b_1 \rightarrow c_2$ , and  $c_1 \rightarrow a_2$ .

<sup>14</sup>B. B. van Aken, Ph.D. thesis, Rijksuniversiteit Groningen, 1973.

<sup>15</sup>C. W. Jones, P. D. Battle, and P. Lightfoot, *Acta Crystallogr., Sect. C: Cryst. Struct. Commun.* **45**, 365 (1989).

<sup>16</sup>P. M. Woodward, *Acta Crystallogr., Sect. B: Struct. Sci.* **53**, 32

(1997).

<sup>17</sup>M. W. Lufaso and P. M. Woodward, *Acta Crystallogr., Sect. B: Struct. Sci.* **60**, 10 (2004).

<sup>18</sup>D. J. Singh, *J. Appl. Phys.* **79**, 4818 (1996).

<sup>19</sup>P. B. Allen, H. Berger, O. Chauvet, L. Forro, T. Jarlborg, A. Junod, B. Revaz, and G. Santi, *Phys. Rev. B* **53**, 4393 (1996).

<sup>20</sup>I. I. Mazin and D. J. Singh, *Phys. Rev. B* **56**, 2556 (1997).

<sup>21</sup>G. Kresse and J. Hafner, *Phys. Rev. B* **47**, R558 (1993).

<sup>22</sup>G. Kresse and J. Furthmüller, *Phys. Rev. B* **54**, 11169 (1995).

<sup>23</sup>G. Kresse and D. Joubert, *Phys. Rev. B* **59**, 1758 (1999).

<sup>24</sup>P. E. Blochl, *Phys. Rev. B* **50**, 17953 (1994).

<sup>25</sup>A group-theoretical analysis shows that the octahedra are not necessarily regular. Howard and Stokes in Ref. 26 write “departures from the regularity are allowed by the space-group symmetry and certainly expected,” though the differences from regular octahedra should be at most second order in the tilt angle. We show in this work that the impact of the octahedron distortions may not be neglected in SrRuO<sub>3</sub>.

<sup>26</sup>C. J. Howard and H. T. Stokes, *Acta Crystallogr., Sect. B: Struct. Sci.* **54**, 782 (1998).

<sup>27</sup>N. Ross, J. Zhao, J. B. Burt, and T. D. Chaplin, *J. Phys.: Condens. Matter* **16**, 5721 (2004).

<sup>28</sup>E. Cockayne and B. P. Burton, *Phys. Rev. B* **62**, 3735 (2000).

<sup>29</sup>T. Kiyama, K. Yoshimura, K. Kosuge, Y. Ikeda, and Y. Bando, *Phys. Rev. B* **54**, R756 (1996).

<sup>30</sup>W. Pies and A. Weiss, in *Crystal Structure Data of Inorganic Compounds*, edited by K.-H. Hellwege and A. M. Hellwege, Landolt-Börnstein New Series, Group III, Vol. 7e (Springer, Berlin, Heidelberg, 1977), p. 8.

<sup>31</sup>R. P. Liferovich and R. H. Mitchell, *J. Solid State Chem.* **177**, 2188 (2004).

<sup>32</sup>N. D. Zakharov, K. M. Satyalakshmi, G. Koren, and D. Hesse, *J. Mater. Res.* **14**, 4385 (1999).

<sup>33</sup>S. C. Gausepohl, M. Lee, K. Char, R. A. Rao, and C. B. Eom, *Phys. Rev. B* **52**, 3459 (1995).

- <sup>34</sup>E. Vasco *et al.*, Adv. Mater. (Weinheim, Ger.) **17**, 281 (2005).
- <sup>35</sup>L. Klein *et al.*, J. Phys.: Condens. Matter **8**, 10111 (1996).
- <sup>36</sup>G. Santi and T. Jarlborg, J. Phys.: Condens. Matter **9**, 9563 (1997).
- <sup>37</sup>R. Kennedy, R. Madden, and P. Stampe, J. Phys. D **34**, 1853 (2001).
- <sup>38</sup>Q. Gan *et al.*, J. Appl. Phys. **85**, 5297 (1999).
- <sup>39</sup>J. Okamoto, T. Mizokawa, A. Fujimori, I. Hase, M. Nohara, H. Takagi, Y. Takeda, and M. Takano, Phys. Rev. B **60**, 2281 (1999).
- <sup>40</sup>K. Johnston, X. Huang, J. B. Neaton, and K. M. Rabe, Phys. Rev. B **71**, 100103(R) (2005).
- <sup>41</sup>J. B. Neaton and K. M. Rabe, Appl. Phys. Lett. **82**, 1586 (2003).
- <sup>42</sup>We continue to refer to this structure as *e-Pbnm* [110] in order to avoid introducing new notation; however, this structure has lower symmetry if the in-plane strain is applied.
- <sup>43</sup>M. Itoh, M. Shikano, and T. Shimura, Phys. Rev. B **51**, 16432 (1995).